CRYSTAL GROWTH & DESIGN

Article

pubs.acs.org/crystal

Effect of Decorating Titanium with Different Self-Assembled Monolayers on the Electrodeposition of Calcium Phosphate

Noah Metoki,[†] Daniel Mandler,*[,‡] and Noam Eliaz*[,†]

[†]Biomaterials and Corrosion Lab, Department of Materials Science and Engineering, Tel-Aviv University, Ramat Aviv 6997801, Israel

[‡]Institute of Chemistry, The Hebrew University of Jerusalem, Jerusalem 9190401, Israel

Supporting Information

ABSTRACT: Calcium phosphate (CaP) ceramics are used in orthopedics and dentistry due to their excellent osseointegration and biocompatibility. The electrodeposition of CaP on titanium alloy covered with self-assembled monolayers (SAMs) was studied with respect to the influence of chain length, end-group charge, and anchoring group. SAMs with end-groups similar to the functional groups on the side chains of collagen were selected. This study is divided to three parts: (1) studying the effects of SAMs on the titanium substrate, (2) studying the process of nucleation and growth of the CaP on specific SAMs, and (3) characterizing the CaP coatings using various surface analytical techniques. It was concluded that the nucleation and growth behavior of CaP changed in the presence of the SAMs. Different surface energies and crystallographic phases were associated with this change. Although the nucleation remained progressive, the growth changed from three-dimensional on bare surfaces to two-dimensional on SAMs-covered surfaces. Moreover, the deposition kinetics was slower on SAMs-covered surfaces, with phases containing a higher Ca/P ratio. Examination of the coating revealed that different SAMs lead to different surface morphologies of the coating while maintaining its degree of crystallinity. Yet, the phase content changes from hydroxyapatite and octacalcium phosphate (HAp + OCP) on the bare electrode to OCP only on the SAMs-covered electrode. These changes may have a substantial effect on the in vivo behavior by changing the coating's solubility and surface morphology, thus affecting cell adhesion, proliferation, and differentiation processes.

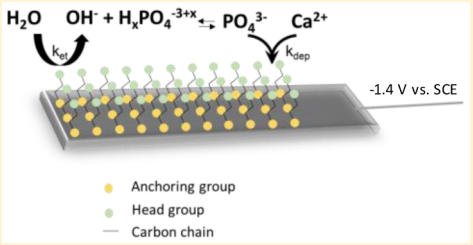

INTRODUCTION

Since their introduction in the 1980s, hydroxyapatite (HAp) coatings on orthopedic implants have gained wide acceptance in orthopedic surgery.[1] It has been repeatedly demonstrated clinically that HAp coatings have osteoconductive properties, and that the fixation of the HAp-coated implants is better than that of uncoated implants following optimal surgical conditions.[2] Research also supports the conclusion that early bone growth and apposition are accelerated by implants coated with HAp.[3−5]

Plasma spraying (PS) is still the most common technology commercially used for depositing HAp coatings onto titanium-based implants. However, PS is a high temperature and line-of-sight process. Potential problems with this technology include exposure of substrates to intense heat, residual thermal stresses, and the inability to coat complex shapes with internal cavities.[6] Thus, other techniques have been explored to address these problems,[7] including ion-beam deposition,[8] chemical deposition,[6] metallo-organic chemical vapor deposition,[9] pulsed laser deposition,[10] and electrophoretic deposition.[11−13]

In this regard, electrochemical deposition (ED) is one of the most promising processes.[14−16] The advantages of ED as compared to PS include (a) good control of the composition and structure of the coatings, (b) relatively low processing temperatures (which enables formation of highly crystalline deposits with low residual stresses and potential incorporation of antibiotics and growth factors in situ), and (c) ability to coat non-line-of-site, porous, or complex surfaces. ED is controlled both by electron transfer and by surface characteristics such as crystallographic phases, orientation, and level of crystallinity.

It is well-known that self-assembled monolayers (SAMs) affect electron transfer as well as the interaction between the deposit and the surface. SAMs are organic monomolecular layers that spontaneously adsorb (chemisorption) onto a surface and form an organized layer. They provide design flexibility, both at the molecular and at the macroscopic level, and offer a quick and easy path of altering electron transfer, and therefore deposition. Previous studies have shown that SAMs strongly affect the crystal growth in various deposits from aqueous solutions. For example, Aizenberg et al.[17] showed that SAMs possessing different end-groups influence the nucleation of calcite ($CaCO_3$). The end-groups of the SAMs induced different nucleation planes, resulting in crystallites of different shapes. Agarwal et al.[18] deposited undoped and Y_2O_3-doped ZrO_2 thin films on SAMs with either sulfonate or methyl terminal groups on single-crystal silicon substrates. The spontaneous deposition of calcium phosphate (CaP) on SAMs has also been studied.[19−24]

Received: January 13, 2016
Revised: April 5, 2016
Published: April 7, 2016

DOI: 10.1021/acs.cgd.6b00057
Cryst. Growth Des. 2016, 16, 2756−2764

Ordinarily, the end-group of the monolayer facing the solution is chosen aiming to mimic the biomineralization process in vivo, where the growth of HAp is associated with the organization of the collagen fibers. Thus, interfacial interactions may exist between HAp and the functional groups on the side-chains of the collagen molecules. Accordingly, several SAMs have been studied, including those with hydroxyl (OH), sulfonic acid (SO_3H), phosphate (PO_4H_2), and carboxyl (COOH) end-groups.[20−23] Some of the negatively charged SAMs were found to be effective in promoting the mineralization process from solution and affected the texture of the CaP coating.[23] There is still a debate in the literature with respect to which SAM is most beneficial for HAp deposition and growth. For example, Liu et al.[20] showed that the crystallization of CaP varied as a function of the SAMs end-group; CaP poorly crystallized on carboxylic and phosphoric acid functional groups and formed an amorphous coating on ethylene and hydroxyl terminal groups.

Several studies focused on the effect of SAMs on coatings prepared by ED. For example, Langerock et al.[25] demonstrated that the thiol-based SAMs markedly altered the nucleation process and growth mechanism of electrodeposited rhodium metal on gold electrodes. Hagenström et al.[26] showed the effect of SAMs on ED by studying the early stages of deposition of Ag on modified Au electrodes. It was found that Ag underpotential deposition onto such surfaces is hindered depending on chain length, but the differences between SAMs with different end-groups are less significant. Malel et al.[27] demonstrated the effect of SAMs with different chain lengths on the deposition of Ag nanoparticles. It was shown that the shape of the nanoparticles was affected by the carbon chain length.

To the best of our knowledge, SAMs have never been studied in the context of CaP electrodeposition. The objective of this research was thus to study the effect of different SAMs, namely, different end-groups and chain lengths, on the surface morphology, phase content, and growth mechanism of ED CaP coatings on titanium alloy. The results will be divided into three main sections: (1) characterization of SAMs on the surface of the titanium alloy, (2) study of the early stages of CaP electrocrystallization on SAMs, and (3) characterization of the CaP coatings.

EXPERIMENTAL SECTION

Preparation of SAMs. 1,3-Propanediol (98%, OH), glutaric acid (99%, CO_2H), butylphosphonic acid (88%, CH_3), 3-aminopropyl-phosphonic acid (98%, NH_2), and (12-phosphonododecyl)-phosphonic acid (97%, 12C) were purchased from Sigma-Aldrich. Propylenediphosphonic acid (95%, 3C) and (6-phosphonohexyl)-phosphonic acid (95%, 6C) were ordered from Sikemia, France. The titanium samples were prepared as described in the Supporting Information. The procedure was similar to that used in our group before.[29] The samples were then immersed in 1 mM solution of the SAM material in DI water for 24 h. This was followed by dipping the samples three times in DI water at ambient temperature and then gently washing them in running DI water.

Characterization of SAMs. Cyclic voltammetry (CV) was conducted in 1 mM $Ru(NH_3)_6Cl_3$ and 0.1 M KNO_3 (98% and 99% respectively, purchased by Sigma-Aldrich) between 0.4 and −0.4 V at a scan rate of 20 mV/s. More details are provided in the Supporting Information. Contact angle measurements were conducted using Ramé-Hart model 100 contact angle goniometer. More details are provided in the Supporting Information. IR spectra were acquired with a Bruker equinox 55 FTIR spectrometer equipped with a mercury cadmium telluride (MCT) detector and coupled with an ATR device. For each spectrum, 2500 scans were collected at a resolution of 4 cm^{-1}. During data acquisition, the spectrometer was continuously purged with dry N_2 to eliminate the spectral contribution of atmospheric water. Electrochemical AFM (Molecular Imaging model PicoSPM) was used to study the initial nucleation and growth of CaP on the different SAMs-covered evaporated titanium surfaces. This system has been used in our group to study the electrochemical processes of nucleation and growth of HAp on Ti.[28] Preparation for contact angle measurements and ATR-FTIR: evaporated samples of titanium (150 nm thick) on glass were treated for 15 min in a UV/ozone apparatus (UVOCS, US). The samples were then modified and further treated as mentioned above.

CaP ED. Preparation of working electrodes for ED was as described in the Supporting Information. The procedure was similar to that used in our group before.[29] The samples were then immersed in 1 mM alkyl chain solution buffered to pH 9 using HCl/Tris buffer for 24 h. This was followed by dipping the samples three times in DI water at ambient temperature and then gently washing them in running DI water.

Electrochemical deposition was carried out with a potentiostat (CHI-750B, CH Instruments Inc., TX, USA). Electrochemical cell: ED was carried out in a standard three-electrode cell (300 mL) in which two graphite rods were used as counter electrodes, a saturated calomel electrode (SCE) was used as the reference electrode, and the sample rod was used as the working electrode. The electrolyte was 0.61 mM $Ca(NO_3)_2$ and 0.36 mM $(NH_4)H_2PO_4$ in DI water.[4,5,30−32] The pH of the bath was measured using an InoLab pH/Oxi Level 3 meter and adjusted to 7.4 by addition of 15 μL of 5 M NaOH before the experiment started. The bath temperature was kept at 37 ± 0.1 °C by means of a WBH-060 Internal & External Circulation Bath. Stirring was carried out at 200 rpm. A PAR-263A potentiostat/galvanostat operating in the potentiostatic mode was used to maintain the cathode potential at −1.4 V vs SCE for 2 h. After ED, the samples were washed in DI water, then soaked in warm DI water (T ∼ 40 °C) for 1 min, and placed in DI water at room temperature in an ultrasonic bath for 2 min. Finally, the samples were dried and stored in a Petri dish sealed in a polyethylene bag.

Characterization of Early Stages of CaP ED. *Chronoamperometry (CA).* The experiment was carried out with a potentiostat (CHI-750B, CH Instruments Inc., TX, USA) and a graphite counter electrode (4.1 cm^2 in area). The working electrode was prepared by embedding 0.2-in. diameter titanium rods in Teflon, cleaning and chemically treating as described above for CV. The current transient under constant voltage of −1.4 V vs SCE was monitored in three solutions. The concentrations of calcium and phosphate ions were changed while keeping the ratio of $[Ca^{2+}]/[PO_4^{3-}]$ = 1.67 and pH = 7.4 constant. The ratio was kept to ensure formation of stoichiometric HAp based on the solubility isotherms of calcium phosphate.[28] Concentration "low" is of the "nominal" solution used in ED (0.61 mM $Ca(NO_3)_2$ and 0.36 mM $(NH_4)H_2PO_4$ in DI water), "medium" is three times that concentration, and "high" is five times the concentration. The ionic strength of the diluted solutions was changed by adding NaCl to match that of the solution with the highest ionic strength. Ionic strength calculations were performed using the PHREEQC geochemical computer program.[31,33] Here, KH_2PO_4 and $CaCl_2$ were used, as opposed to $Ca(NO_3)_2$ and $(NH_4)H_2PO_4$ used in the electrochemical cell, in order to avoid the contribution of nitrate ions to the electrochemical process.

In Situ AFM. The exposed area of the working electrode was 1 cm^2 in the AFM liquid cell, which contained 0.5 mL of solution prepared as specified before for the ED. A Pt wire was used as a counter and as a quasi-reference electrode.[28] The liquid cell was kept at constant temperature of T = 37 °C by means of LakeShore 321 Autotuning temperature controller. An EG&G/PAR (Princeton, NJ) model 263A potentiostat/galvanostat operating in the potentiostatic mode was attached to the AFM cell and employed to maintain the cathode potential at the equivalent of −1.4 V vs SCE.

TOF-SIMS. TOF-SIMS data were acquired using a TOF SIMS5 instrument (ION-TOF GmbH, Germany). The primary ion beam used was Bi_1^+ in the static mode. The ion dose in each experiment was 2×10^{12} primary ions/cm^2. The analyzed area was 200 × 200 μm^2. Ti-

DOI: 10.1021/acs.cgd.6b00057
Cryst. Growth Des. 2016, 16, 2756−2764

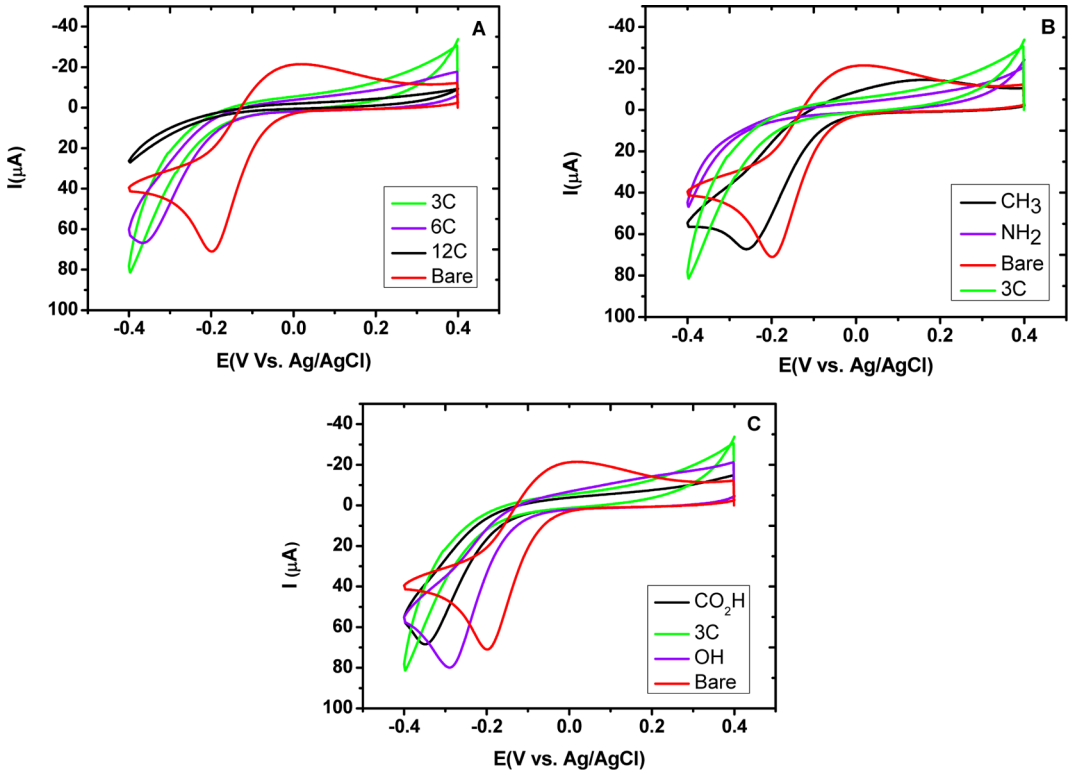

Figure 1. CV of Ti electrodes recorded at a scan rate of 20 $mV \cdot s^{-1}$ in a solution consisted of 1 mM $Ru(NH_3)_6^{3+}$ and 0.1 M KCl. (A) The effect of chain length; (B) the effect of the end-group charge; (C) the effect of α,ω anchoring groups.

6Al-4V samples used for the ED were cleaned and modified as described before with respect to CV experiments.

Roughness parameters were calculated following image processing with the aid of SPIP software.[30]

Characterization of the Final Coating. X-ray photoelectron spectroscopy (XPS) spectra were recorded using an Axis Ultra spectrometer (Kratos), and Mg−Kα radiation of 1486.71 eV. Data were collected and analyzed by a Vision processing program. The surface morphology was revealed in an environmental scanning electron microscope (ESEM, Quanta 200 FEG, FEI). X-ray diffraction (XRD) scans were acquired using a Scintag powder diffractometer within the range of 2θ = 0−100° at a scan rate of 0.05 deg/s. They allowed determining the phase content in the coating.

RESULTS AND DISCUSSION

Preparation of SAMs and their Characterization. We studied the following parameters:

(1) Chain length: Molecules with equivalent end-groups, i.e., PO_3H_2-$(CH_2)_n$-PO_3H_2 (n = 3, 6, or 12).
(2) End-group charge: Three propylene chains with phosphonic acid at one end and either positive, negative or neutral functional group at the other end, i.e., PO_3H_2-$(CH_2)_3$-x (x = PO_3H_2, NH_2, CH_3).
(3) Anchoring group: Three propylene chains with two identical α,ω-functional groups of the formula y-$(CH_2)_3$-y, where y = PO_3H_2, COOH, or OH.

First, we examined the formation of the different SAMs on the titanium surface by means of chemisorption. The formation was monitored using CV (Figure 1) and contact angle (θ) measurements (Table 1). Figure 1 shows the CV of $Ru(NH_3)_6^{3+}$ carried out with the different SAMs. In general, the monolayers clearly exhibit a partially blocking behavior of electron transfer as compared with the bare titanium alloy. Blocking was estimated by the decrease of the peak current

Table 1. Average Contact Angle Values (n = 3) of Bare and Chemisorbed SAMs on Titanium Surface

SAM abbreviation	advancing contact angle deg ±0.1°	receding contact angle deg ±0.1°
bare	24.7 ± 0.7	9.4 ± 2.2
3C	10.9 ± 1.8	
6C	16.8 ± 5.0	
12C	53.3 ± 18.4	39.9 ± 15.1
OH	8.5 ± 3.0	
COOH	12.6 ± 6.6	
CH_3	68.1 ± 0.6	50.6 ± 0.5
NH_2	9.2 ± 1.9	

(measured at the peak potential) and compared with that of a bare electrode. Figure 1A shows the effect of the chain length using α,ω-alkyl diphosphonic acid monolayers. A lower rate of electron transfer with growing chain length can be seen and is in agreement with previous reports.[34] This clearly suggests that the monolayers do not lie parallel to the surface, yet even the (12-phosphonododecyl)phosphonic acid (12C) is not highly organized as it does not fully block electron transfer. Figure 1B shows the effect of the functional group pointing to the solution. Three different groups were examined: methyl (CH_3), amino (NH_2), and phosphonic acid (3C). Clearly, the functional group affects the charge transfer at the interface. The NH_2 slows down electron transfer, presumably due to the positive charge, which repels the positively charged ruthenium complex. The effect of the negatively charged 3C is not completely clear as it is expected to attract the positively charged complex. We speculate that it is the negative potential applied to the electrode which affects the organization of the 3C, repelling it from the surface and therefore increasing its blocking properties as compared to the uncharged CH_3.

DOI: 10.1021/acs.cgd.6b00057
Cryst. Growth Des. 2016, 16, 2756−2764

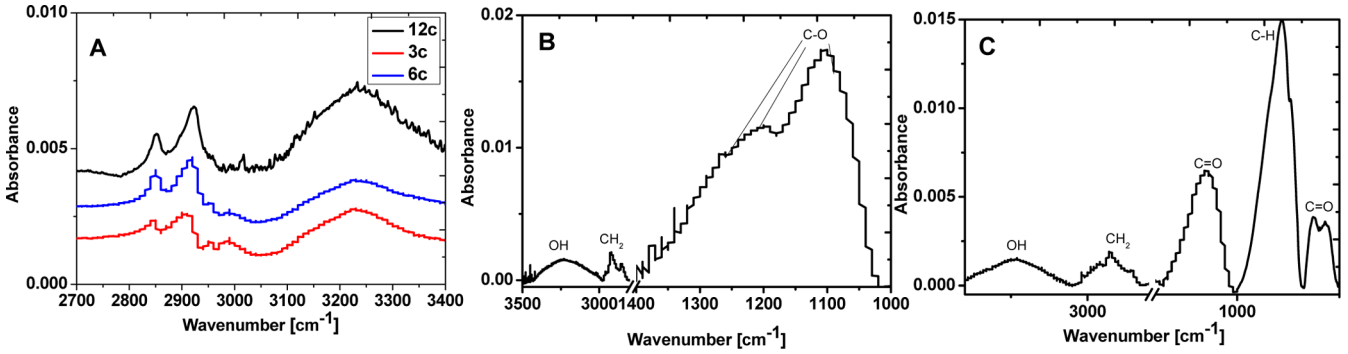

Figure 2. ATR-FTIR spectra of the various SAMs on titanium: (A) 3C, 6C, 12C; (B) OH; and (C) CO_2H.

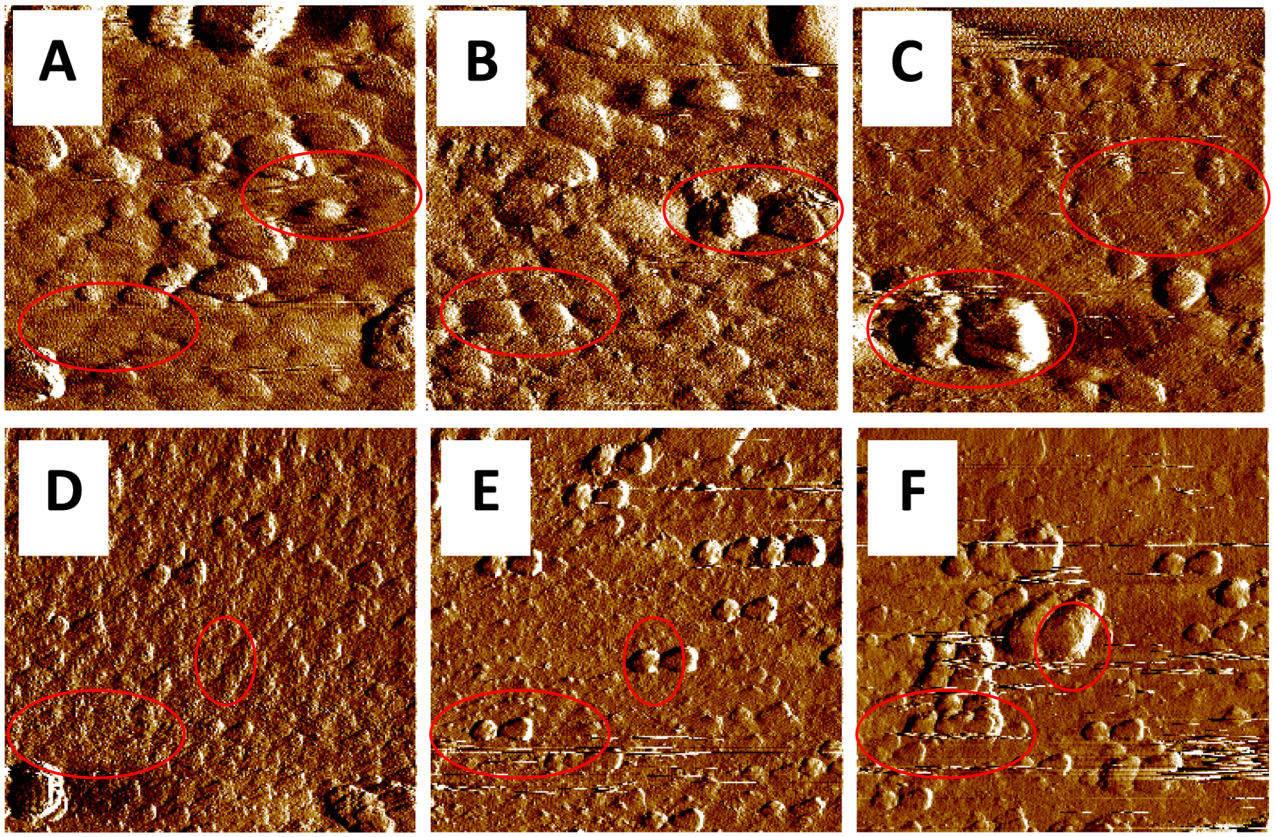

Figure 3. In-situ EC-AFM deflection images of bare (A, B, C) and CH_3-covered (D, E, F) surfaces at open circuit, 3 or 5 min potentiostatic deposition of CaP. All images are 2 × 2 μm^2.

Furthermore, the three carbon chains are usually not closely packed, which also contributes to the facile charge transfer. Figure 1C shows the CV obtained with y-$(CH_2)_3$-y (y = PO_3H_2, CO_2H, OH) SAMs. It can be seen that the rate of electron transfer decreases in the following order: OH > CO_2H > PO_3H_2. This can be attributed to the affinity between the functional group of the SAM and the titanium oxide surface. The lower the affinity is, the higher the electron transfer is. As expected, the hydroxyl group shows the weakest attachment to the surface as it is only physically adsorbed. The weakly bonded hydroxyl group is followed by the carboxylic acid, and finally the phosphonic acid that shows the highest bonding strength, as previously reported.[35]

Contact angle measurements can help in deducing which of the SAMs are more ordered and packed, as demonstrated in our previous publication.[34] The effect of the alkyl chain length (3C, 6C, and 12C) follows the expected trend of increasing hydrophobicity with chain length. Note that contact angle measurements of very hydrophilic SAMs (θ < 24°) are not reported to have a receding contact angle as the difference between the receding and advancing contact angle was difficult to measure. The effect of the functional group can be seen, as both the positive and the negative functional groups induce hydrophilic surfaces. These bear little difference following the polarizability of water. In contrast, the CH_3 group has no charge, leading to a hydrophobic surface.

When compared to data reported before, CH_3 and NH_2 gave rise to relatively low values,[23] although still reflecting the hydrophilic/hydrophobic nature of these SAMs. The values should be in the range of 102−110° and 25−37°, respectively.[23] The difference must be attributed to the different substrates, i.e., titanium vs gold. With regard to glutaric acid (CO_2H) and

DOI: 10.1021/acs.cgd.6b00057
Cryst. Growth Des. 2016, 16, 2756−2764

propanediol (OH), the literature shows hydrophilic surfaces similar to those observed here.[23]

Further characterization of the surfaces coated with SAMs was carried out by means of ATR-FTIR spectroscopy. Figure 2A shows the spectra of alkyl diphosphonic acid with different chain lengths. In all spectra, peaks associated with the methylene symmetric $\upsilon_s(-CH_2)$ and asymmetric $\upsilon_{as}(-CH_2)$ stretching modes are visible at ca. 2850 and 2920 cm^{-1}, respectively, indicating the presence of aliphatic chains at the titanium surface. The methylene stretching modes are known to be sensitive to the conformational order of the alkyl chains (gauche defects), shifting to higher frequencies with increasing conformational disorder.[34] The 12 carbon chain (12C) shows a shift to higher frequencies of 2851 and 2924 cm^{-1}, indicating a disordered monolayer. The peaks of the methylene vibrations of the shorter chains (3C and 6C) cannot be accurately determined due to their low intensity. The broad band at higher frequencies, i.e., > 3000 cm^{-1}, is attributed to adsorbed water.

Figure 2B shows the spectrum typical of OH SAM on titanium. Distinct peaks are seen for the OH, CH_2, and C−O bonds. The C−O stretching bond is of strong intensity and shows both C−O stretching and C−OH bending modes.[36] Figure 2C of CO_2H SAM on titanium surface shows a different spectrum, with strong intensities associated with the C═O bond.[36]

Characterization of the Early Stages of CaP Electrodeposition. Figure 3A−C and D−F presents 2 × 2 μm^2 in situ AFM deflection mode images of bare and CH_3-covered evaporated-titanium surfaces, respectively. The deflection image represents a gradient of shape change, and thus, it is more sensitive to surface topography and composition than topography imaging. The images were acquired at different stages of the experiment: (A, D) under open-circuit potential, (B, E) and (C, F) after potentiostatic deposition at E_{dep} = −1.4 V vs SCE for 3 and 5 min, respectively. The red circles mark CaP nuclei. Comparing between surfaces at their rest potential (Figure 3A,D), it is evident that the surface topography changes following coverage with CH_3−SAMs. The average roughness of three measurements is R_a = 46.0 ± 1.9 nm for bare Ti, and 41.7 ± 0.1 nm for covered CH_3−SAM. Thus, the addition of SAMs makes the surface slightly smoother.

Distinct differences can be seen upon CaP growth between the bare surface and that covered with a SAM (Figure 3, B vs E and C vs F). The electrocrystallization of CaP on the bare Ti surface is characterized by larger islands (3D growth). In contrast, the electrocrystallization of CaP on a CH_3-covered surface exhibits smaller islands that grow laterally (2D growth).

The most important parameters determining the mode of growth of a substance on a foreign substrate are the deposit/substrate binding energy and the crystallographic match between them.[28] Therefore, it is not surprising that the growth changes in the presence of SAMs. The crystallographic structure of both titanium and HAp is hcp. Yet, we recall that HAp deposits on the titania, which has a different structure (e.g., amorphous or tetragonal).[37] It has been reported that the anatase phase is much more efficient in nucleation and growth of HAp (bone growth) than the rutile phase, presumably because of the better lattice match with the HAp phase.[38] We do not know the crystallographic structure that the SAMs form on titania, which does not necessarily match that on Au (the latter being hexagonal).[39] While it seems that the nucleation can be determined as progressive for both substrates (because the surface sites are not converted immediately into nuclei), the growth mode seems to be different. Evidently, the binding energy between the coating and the substrate changes significantly due to the SAM. The bare surface has hydroxyl groups interacting with the solution, while the SAM-covered substrate has hydrophobic methyl groups. This is evident in Table 1, showing that the bare surface is much more hydrophilic than the SAM-covered substrate. In the case that the binding energy between the adsorbed deposited ions is higher than that between the adsorbed ion and the substrate, three-dimensional islands are anticipated according to Volmer−Weber model. For the opposite case, i.e., when the binding energy between the adsorbed deposited ions is lower than that between the adsorbed ions and the substrate, and the crystallographic misfit is significant, formation of strained two-dimensional layers is followed by unstrained three-dimensional islands according to the Stranski−Krastanov model.[28]

Chronoamperometry (CA) was carried out on titanium surfaces in order to better understand the initial film growth. As shown before, CaP growth on the titanium electrode surfaces is a very complex process.[16,28,31,40] The latter includes mainly three parts: (1) local electrochemical reactions, which increase the pH within the diffusion layer; (2) dissociation of phosphoric acid; and (3) CaP electrocrystallization on the electrode surface. The latter behaves differently than conventional electrodeposition of metals, and may be associated with precipitation in solution and electrophoretic attraction.[28,31] The whole process is depicted in Scheme 1. As this process is complex, the current transient cannot be directly related to the deposition stage.

Scheme 1. Electrodeposition Process of CaP, where k_{et} is the Rate Reaction Constant of Water Reduction and k_{dep} is the Rate Reaction Constant of CaP Deposition

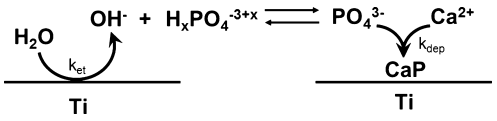

Hence, we investigated the CA of bare Ti surface and that modified by CH_3 or CO_2H SAMs. A set of CA measurements was performed, maintaining the ionic strength (by adding NaCl), pH, and the ratio of the Ca/P ions ratio in solution constant, while changing calcium and phosphate concentrations. Specifically, we employed three concentrations of Ca and P, denoted hereafter low (0.61 mM and 0.36 mM, respectively), medium (1.83 mM and 1.08 mM, respectively), and high (3.05 mM and 1.8 mM, respectively). Before dealing with the CA, it is important to notice that the cathodic current originates mainly from the reduction of water.[16,28,31,40] This has been calculated previously by Eliaz et al.[28] The reduction of water generates hydroxyl ions, which can be consumed by the hydrogen phosphate species, causing it to deprotonate and associate with Ca^{2+}. Hence, the current is expected to increase in case that the hydroxyl ions are consumed very fast, shifting the electrochemical reduction process as in an EC mechanism.[16,28,31,40] This is indeed observed for a bare electrode: Figure 4A shows a clear increase in the cathodic current as the concentrations of the Ca and P species in solution are increased, thus indicating faster kinetics of the chemical coupled processes. However, the difference is not high, possibly

DOI: 10.1021/acs.cgd.6b00057
Cryst. Growth Des. 2016, 16, 2756−2764

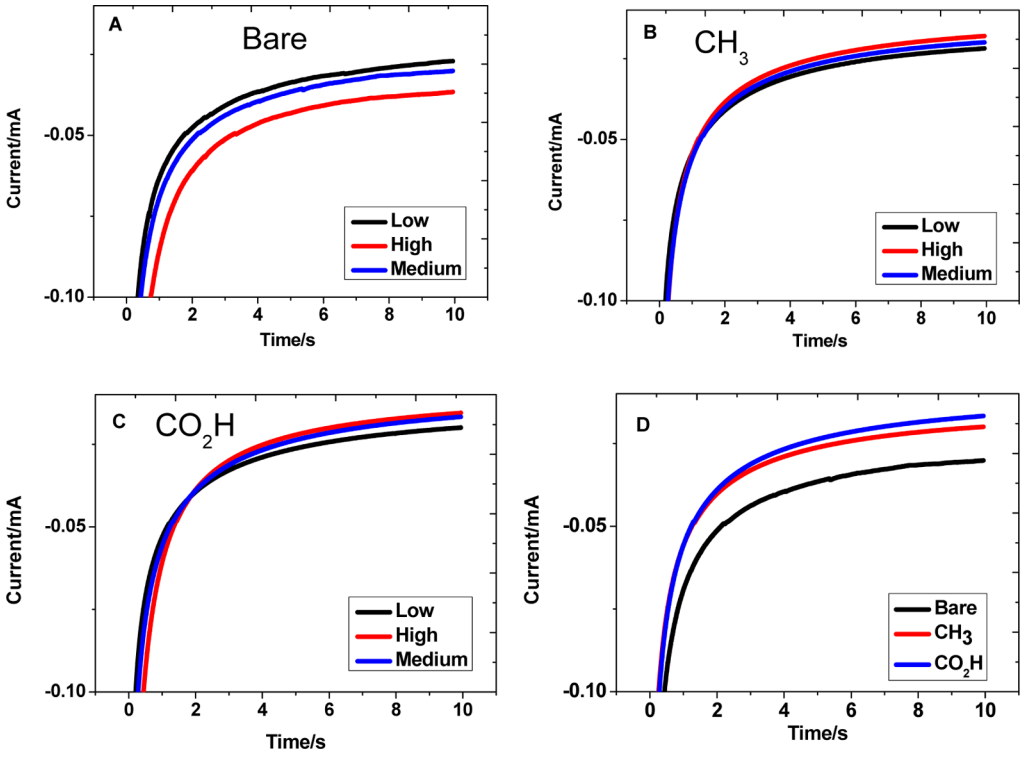

Figure 4. CA for bare (A), CH_3-modified (B), and COOH-modified (C) surfaces in CaP solutions of different concentrations. (D) Shows the comparison between the three surfaces for the same solution concentration (medium).

because within this time frame, the nucleation is nonuniform, i.e., progressive as revealed by in situ, real-time AFM. It is evident that the CA of bare titanium is different than that of Ti coated with SAMs (Figure 4B,C). The effect of increasing the concentration of Ca and P species is minor for the coated surfaces. This suggests that in the presence of the SAMs the consumption of hydroxyl ions is not affected by increasing the concentration of the precipitating ions. A plausible explanation is that the organic monolayers slow down the precipitation of CaP.

The composition and pH of the electrolyte is also important. It has been reported that when the electrolyte is under a lower level of supersaturation (e.g., lower concentration of OH^-) heterogeneous nucleation and growth of HAp on titanium dominates and the crystals grow larger, whereas at higher level of supersaturation with respect to HAp homogeneous nucleation dominates.[41]

It is somewhat surprising that the CA is indifferent to the functional end-group of the SAM as opposed to the chemical precipitation of calcium phosphate.[28,24,42,43] We speculate that the concentrations of the Ca and P are insufficient to affect significantly the concentration of hydroxyl ions when the surface is coated with a SAM. Figure 4D shows that for a given concentration of Ca and P species (i.e., medium concentration) the currents of Ti coated with SAMs are lower than that of bare titanium. This might be due to either decreasing the rate of electron transfer for the SAMs-coated surfaces or to the slow consumption of the hydroxyl ions by the slow precipitation of CaP on the SAMs.[34] It is worth mentioning that the current transients on bare and SAMs-coated Ti merge after 10−15 min. This is understandable due to the buildup of a relatively thick (compared to the SAM) CaP layer, which eventually governs the rate of electron transfer.

TOF-SIMS was applied to obtain information about the early phase content of the coating. This included determination of the ratios of PO_3^-/PO_2^- emitted from the substrate upon bombardment with Bi_1^+ in the static mode. This technique is sensitive to small amounts of material on the surface. The PO_3^-/PO_2^- ratio is a well-known characteristic of CaP phases.[24,44] Table 2 summarizes the ratios obtained for

Table 2. PO_3^-/PO_2^- and Ca/P Ratios Obtained from TOF-SIMS Studies of Bare and SAMs-Covered Titanium Alloy Electrodeposited with CaP for 3 min

	HAp	β-TCP	OCP	bare	CH_3-covered titanium	CO_2H-covered titanium
PO_3^-/PO_2^-	0.404	0.352	0.719	1.013	0.335	0.610

commercial (HAp and TCP) and synthesized powders (OCP)[45] as well as titanium samples electrodeposited for 3 min. The values obtained for the powders are similar to those previously reported.[24,43] Nevertheless, there are many phases that were not analyzed here, such as dicalcium phosphate dihydrate (DCPD), dibasic calcium phosphate (DCP), and monocalcium phosphate (MCP), and are known to have higher ratios of PO_3^-/PO_2^-.[44] While these ratios are required to interpret the values experimentally obtained for the bare electrode, it should be emphasized that the values must be obtained under exactly the same experimental conditions.[44] Hence, values reported previously must be handled cautiously when drawing conclusions concerning our results. Nevertheless, the values reported by Lu et al.[44] for reference powders are similar to ours for a bare electrode. Lu et al.[44] also examined other phases of CaP, including DCPD (1.15 ± 0.07), DCP (1.22 ± 0.05), and MCP (2.33 ± 0.11). Therefore, in spite of

DOI: 10.1021/acs.cgd.6b00057
Cryst. Growth Des. 2016, 16, 2756−2764

Table 3. Chemical Composition (atom %) of the CaP-Coated Titanium Samples Covered with Different SAMs, as Determined by High-Resolution XPS Scans

element	CO_2H	3C	6C	12C	OH	CH_3	NH_2
C	12.58	15.70	12.11	12.05	13.15	12.72	10.25
O	57.13	55.54	57.16	57.93	57.02	56.59	58.05
Ca	16.98	16.39	17.52	17.23	17.04	17.29	17.96
P	13.30	12.36	13.22	12.79	12.78	13.40	13.75
Ca:P	1.28	1.33	1.33	1.35	1.33	1.29	1.31
O:Ca	3.36	3.39	3.26	3.36	3.35	3.27	3.23
$O(1s)_{II}/O(1s)$	0.049	0.057	0.056	0.057	0.057	0.059	0.057
$Ca:P_{adjusted}$	1.24	1.29	1.29	1.31	1.33	1.25	1.28
$O:Ca_{adjusted}$	3.31	3.33	3.21	3.31	3.29	3.22	3.19
$O(1s)_{II}/O(1s)_{adjusted}$	0.049	0.058	0.057	0.049	0.058	0.060	0.058

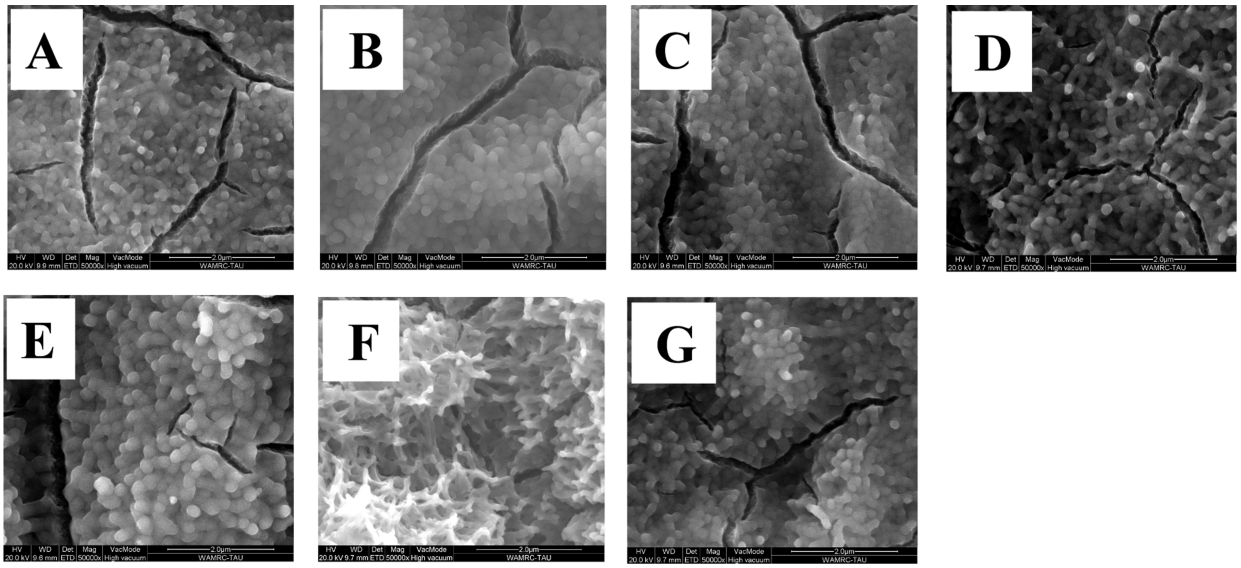

Figure 5. SEM images of the "nominal" CaP coating pretreated with (A) 3C, (B) 6C, (C) 12C, (D) NH_2, (E) CO_2H, (F) CH_3, and (G) OH SAMs.

the fact that a conclusive analysis cannot be made, we suggest that the deposit on the bare electrode is presumably made of a mixture of OCP and one of the above phases.

From Table 2 it is apparent that the surfaces coated with a SAM have PO_3^-/PO_2^- values closer to the phases of higher calcium content, i.e., OCP, HAp, and TCP. The latter are FDA approved.[33] Thus, the coating obtained on top of the SAMs after a short deposition time consists of the desired phases, as opposed to that on a bare surface, which is similar to a precursor phase such as DCPD.[44]

Characterization of the Final CaP Coatings. Low-resolution XPS survey spectra (not shown) from all samples revealed Ca, P, and O from the CaP coating and C from carbonate contaminations on the surface. Traces of Ti were also detected (<0.8%) in some of the samples, which are attributed either to a thin or to a very porous coating. Fluorine impurity (<0.5%) was also detected and may be associated with the surface pretreatment with HF. The atomic concentrations of the elements obtained from high-resolution XPS measurements, together with the Ca/P and O/Ca atomic ratios, are shown in Table 3. For comparison, the theoretical Ca/P ratios are 1.00, 1.33, 1.50, 1.50, and 1.67 for DCPD, OCP, amorphous calcium phosphate (ACP), TCP, and HAp, respectively,[44] and the theoretical O/Ca ratios for these phases are 6.00, 3.125, 3.00, 2.67, and 2.60, respectively.[44] The measured Ca/P and O/Ca ratios for all samples fit best the theoretical values of the OCP phase alone. The measured Ca/P atomic ratio obtained from conventional XPS analysis has been reported to be always lower than the theoretical value for different calcium phosphates on the surface, thus preventing their unambiguous identification.[44] Therefore, in order to identify the phases conclusively, the oxygen loss spectrum was analyzed. The values of $O(1s)_{II}/O(1s)$ are also provided in Table 3. In comparison, Lu et al.[44] and Metoki et al.[33] measured mean $O(1s)_{II}/O(1s)$ ratios of 0.072, 0.065, 0.053, 0.037, 0.020, and 0.008 for powders of TCP, HAp, OCP, dibasic calcium phosphate anhydrous (DCPA), DCPD, and monobasic calcium phosphate monohydrate (MCPM), respectively. Thus, the measured values reported in Table 3 all fall within the values previously reported as typical of OCP. The "adjusted" values provided in Table 3 are adjusted to carbonate contamination in the coating that substitutes the PO_4^{3-} ions. The adjusted values correspond well with the previously reported value for pure OCP. In comparison, the coating deposited from the "nominal" solution on a bare surface was previously reported to consist of 50% HAp and 50% OCP.[33] These results suggest that the presence of a SAM causes a significant change in phase content formed by electrochemical deposition. This is in accordance with the TOF-SIMS results, which indicated that the preliminary phase precipitated on the titanium coated with SAMs is no longer a precursor, but a more crystallized phase such as TCP or OCP.

DOI: 10.1021/acs.cgd.6b00057
Cryst. Growth Des. 2016, 16, 2756−2764

Figure 5 shows SEM images of different CaP coatings deposited on SAMs. The Ca/P ratio based on EDS analysis yields a range between 1.68 and 1.87, indicating on potentially different phase content. Yet, it should be noted that EDS analysis is unreliable for electrodeposited CaP,[40] in contrast to the advanced XPS analysis. Figure 5 indicates that although the phase content was essentially the same for different SAMs, the surface morphology of the CaP coating changed significantly. Figure 5A shows the typical surface morphology of the "nominal" coating. This coating is fairly uniform and contains cracks that had probably formed during the pretreatment stage.[30] The substrate is covered by a dense CaP film composed of globules of approximately 100 nm in size. As shown above, the growth mechanism is affected by the presence of the SAMs and their functional group, which is also likely to influence the surface morphology. It can be seen that the globules appearing at the surface of the "nominal" coating change in shape and size as the underline SAMs changes. For example, the CaP electrochemically deposited on a surface modified by CH_3 yields a unique morphology (Figure 5F). This may be attributed to the lack of charge of this SAM, which affects and screens the interaction between the CaP and the surface. It is widely believed that the *in vivo* behavior of the CaP coating can be greatly affected by its structural parameters such as phase content, texture, crystal size, surface morphology, size and distribution of pores, etc.[40] Therefore, the different coatings presented in this figure are likely to perform differently *in vivo*. The thickness of the coating was measured for two out of the six surfaces coated with SAMs: CO_2H and CH_3. It was found that the thickness of the coating decreased from 4.9 ± 2.4 μm[33] on the bare titanium to 0.8 ± 0.1 and 1.1 ± 0.3 μm for CH_3 and CO_2H, respectively. We attribute this to the effect of the SAMs on the rate of electron transfer.[46]

Figure 6 compares typical XRD spectra for CaP coatings deposited on top of different SAMs (CH_3, CO_2H, and 3C). All

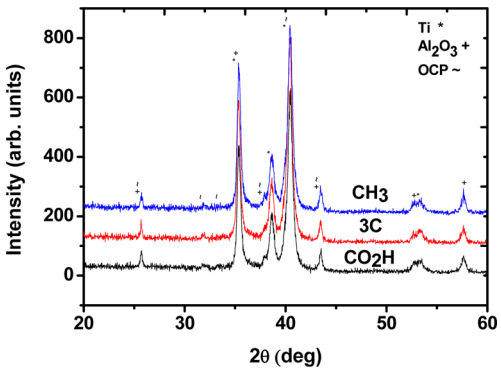

Figure 6. XRD patterns showing that single-phase OCP coating formed under near-physiological conditions on SAMs-coated titanium substrate grit blasted with alumina.

reflections are assigned to OCP, alumina, and the base metal, but not to any other CaP phase (reflections confirmed with JCPDS 04-003-557 for titanium, 97-003-1546 for alumina, and 44-0778 for OCP). The peaks seem to be similar for different samples, thus indicating that the level of crystallinity of these three coatings is similar. Moreover, the ratio between the strongest reflection of the coating and that of the substrate is similar for the three samples, suggesting comparable thickness, as confirmed earlier for two out of the three samples.

CONCLUSIONS

SAMs with different chain lengths, end-group charge, and anchoring groups were assembled on Ti-6Al-4V via chemisorption. The bare and modified titanium alloys were studied by various surface techniques. It was found that (1) long-chain acids form close-packed monolayers, resulting in more hydrophobic surfaces. Furthermore, the longer the chain, the more significant is the reduction of electron transfer across the interface. (2) The charge of the end-group influences the behavior of electron transfer under applied potential and hydrophobicity. (3) The affinity of the anchoring group to the surface also affects electron transfer.

Studying the early stages of the electrochemically assisted nucleation and growth of calcium phosphate revealed that the surface energy and crystallographic structure affect the growth mode, in agreement with previous studies. Although the nucleation type remained progressive, the growth mode changed from 3D on bare surfaces to 2D on SAMs-covered surfaces. Moreover, TOF-SIMS showed that Ca-rich phases are formed initially in the presence of the SAMs, in contrast to the precursors that first grow on bare surfaces.

SEM, XPS, and XRD analyses showed different surface morphologies but similar thicknesses and level of crystallinity for different CaP coatings. It is concluded that the surface morphology of the coating is influenced by the SAM's end-group, and therefore it is likely to influence the coating's behavior in the human body. All coatings grown on SAMs consist of OCP only, as opposed to a coating consisting of both OCP and HAp that was obtained on a bare Ti surface. This may also have a substantial influence on the in vivo behavior. In addition, the SAMs in this work were chosen with an end-group, which is similar to the functional groups on the side-chains of the collagen molecules. Therefore, they may mimic the biomineralization process in vivo, thus greatly enhancing osseointegration and leading to a faster path of patient recovery.

ASSOCIATED CONTENT

Supporting Information

The Supporting Information is available free of charge on the ACS Publications website at DOI: 10.1021/acs.cgd.6b00057.

Experimental section; preparation of SAMs, characterization of SAMs, CaP ED (PDF)

AUTHOR INFORMATION

Corresponding Authors

*Phone: +972-2-658-5831. Fax: +972-2-658-5319. E-mail: daniel.mandler@mail.huji.ac.il.

*Phone: +972-3-640-7384. Fax: +972-3-640-6648. E-mail: neliaz@tau.ac.il.

Notes

The authors declare no competing financial interest.

ACKNOWLEDGMENTS

This study was financially supported by a Kamin Grant 52694-5 from the Israel Ministry of Economy. The partial support by the Focal Technology Area through the Israel National Nanotechnology Initiative (INNI) is acknowledged. The authors thank Dr. Yuri Rosenberg and Dr. Larisa Burstein from the Wolfson Applied Materials Research Centre at Tel-Aviv University for their XRD and XPS characterization service,

DOI: 10.1021/acs.cgd.6b00057
Cryst. Growth Des. 2016, 16, 2756−2764

respectively. We are also grateful to Dr. Catherine Cytermann from the Surface Science Laboratory at the Technion − Israel Institute of Technology, for the TOF-SIMS characterization. Dr. Sofiya Kolusheva from the Ilse Katz Institute for Nanoscale Science and Technology at Ben-Gurion University of the Negev is also acknowledged for her assistance in ATR-FTIR characterization. We thank also Mr. Levinshtein for his technical assistance.

■ ABBREVIATIONS

CaP, calcium phosphate; self-assembled monolayers, SAMs; HAp, hydroxyapatite; OCP, octacalcium phosphate; PS, plasma spray; ED, electrochemical deposition; OH, 1,3-propanediol; CO_2H, glutaric acid; CH_3, butylphosphonic acid; NH_2, 3-aminopropylphosphonic acid; 12C, (12-phosphonododecyl)-phosphonic acid; 3C, propylenediphosphonic acid; 6C, (6-phosphonohexyl)phosphonic acid; CV, cyclic voltammetry; RE, reference electrode; DI, deionized; FTIR, Fourier transform infrared; MCT, mercury cadmium telluride; ATR, atennuated total reflection; AFM, atomic force microscope; GB, grit blasting; SCE, started calomel electrode; CA, chronoamperometry; TOF SIMS, time-of-flight secondary ion mass spectroscopy; XPS, X-ray photoelectron spectroscopy; XRD, X-ray diffraction; ESEM, environmental scanning electron microscopy; SEM, scanning electron microscopy; Ti, titanium; TCP, tricalciumphosphate; DCPD, dicalcium phosphate dehydrate; DCP, dibasic calcium phosphate; MCP, monocalcium phosphate; FDA, Food and Drug Administration; ACP, amorphous calcium phosphate; DCPA, dibasic calcium phosphate anhydrous; MCPM, monobasic calcium phosphate monohydrate

■ REFERENCES

(1) Overgaard, S. *Acta Orthop. Scand.* **2000**, *71*, 1−74.
(2) Soballe, K.; Hansen, E. S.; Rasmussen, H. B.; Jorgensen, P. H.; Bunger, C. *J. Orthop. Res.* **1992**, *10*, 285−299.
(3) Thomas, K. A.; Cook, S. D.; Haddad, R. J.; Kay, J. F.; Jarcho, M. *J. Arthroplasty* **1989**, *4*, 43−53.
(4) Wang, H.; Eliaz, N.; Xiang, Z.; Hsu, H. P.; Spector, M.; Hobbs, L. W. *Biomaterials* **2006**, *27*, 4192−4203.
(5) Lakstein, D.; Kopelovitch, W.; Barkay, Z.; Bahaa, M.; Hendel, D.; Eliaz, N. *Acta Biomater.* **2009**, *5*, 2258−2269.
(6) Wen, H. B.; de-Wijn, J. R.; Cui, F. Z.; de-Groot, K. *J. Biomed. Mater. Res.* **1998**, *41*, 227−236.
(7) Suchanek, W.; Yoshimura, M. *J. Mater. Res.* **1998**, *13*, 94−117.
(8) Luo, Z. S.; Cui, F. Z.; Li, W. Z. *J. Biomed. Mater. Res.* **1999**, *46*, 80−86.
(9) Spoto, G.; Ciliberto, E.; Allen, G. C. *J. Mater. Chem.* **1994**, *4*, 1849−1850.
(10) Tucker, B. E.; Cottell, C. M.; Auyeungt, R. C.; Spector, M.; Nancollas, G. H. *Biomaterials* **1996**, *17*, 631−637.
(11) Ducheyne, P.; Radin, S.; Heughebaert, M.; Heughebaert, J. C. *Biomaterials* **1990**, *11*, 244−254.
(12) Sridhar, T. M.; Eliaz, N.; Kamachi Mudali, U.; Baldev, R. *Corros. Rev.* **2002**, *20*, 255−293.
(13) Eliaz, N.; Sridhar, T. M.; Kamachi Mudali, U.; Baldev, R. *Surf. Eng.* **2005**, *21*, 238−242.
(14) Shirkhanzadeh, M. *J. Mater. Sci.: Mater. Med.* **1995**, *6*, 90−93.
(15) Shirkhanzadeh, M. *J. Mater. Sci. Lett.* **1991**, *10*, 1415−1417.
(16) Eliaz, N. *Isr. J. Chem.* **2008**, *48*, 159−168.
(17) Aizenberg, J.; Black, A. J.; Whitesides, G. M. *Nature* **1999**, *398*, 495−498.
(18) Agarwal, M.; Guire, M. R.; Heuer, A. H. *J. Am. Ceram. Soc.* **1997**, *80*, L2967−L2981.
(19) Li, H.; Huang, W.; Zhang, Y.; Zhong, M. *Mater. Sci. Eng., C* **2007**, *27*, 756−761.
(20) Liu, Q.; Ding, J.; Mante, F. K.; Wunder, S. L.; Baran, G. R. *Biomaterials* **2002**, *23*, 3103−3111.
(21) Liu, D. P.; Majewski, P.; O'Neill, B. K.; Ngothai, Y.; Colby, C. B. *J. Biomed. Mater. Res., Part A* **2006**, *77*, 763−772.
(22) Majewski, P. J.; Allidi, G. *Mater. Sci. Eng., A* **2006**, *420*, 13−20.
(23) Tanahashi, M.; Matsuda, T. *J. Biomed. Mater. Res.* **1997**, *34*, 305−315.
(24) Tarasevich, B. J.; Chusuei, C. C.; Allara, D. L. *J. Phys. Chem. B* **2003**, *107*, 10367−10377.
(25) Langerock, S.; Ménard, H.; Rowntree, P.; Heerman, L. *Langmuir* **2005**, *21*, 5124−5133.
(26) Hagenström, H.; Esplandiú, M. J.; Kolb, D. M. *Langmuir* **2001**, *17*, 839−848.
(27) Malel, E.; Colleran, J.; Mandler, D. *Electrochim. Acta* **2011**, *56* (20), 6954−6961.
(28) Eliaz, N.; Eliyahu, M. *J. Biomed. Mater. Res., Part A* **2007**, *80*, 621−634.
(29) Eliaz, N.; Ritman-Hertz, O.; Aronov, D.; Weinberg, E.; Shenhar, Y.; Rosenman, G.; Weinreb, M.; Ron, E. *J. Mater. Sci.: Mater. Med.* **2011**, *22*, 1741−1752.
(30) Eliaz, N.; Shmueli, S.; Shur, I.; Benayahu, D.; Aronov, D.; Rosenman, G. *Acta Biomater.* **2009**, *5*, 3178−3191.
(31) Eliaz, N.; Sridhar, T. M. *Cryst. Growth Des.* **2008**, *8*, 3965−3977.
(32) Wang, H.; Eliaz, N.; Hobbs, L. W. *Mater. Lett.* **2011**, *65*, 2455−2457.
(33) Metoki, N.; Leifenberg-Kuznits, L.; Kopelovich, W.; Burstein, L.; Gozin, M.; Eliaz, N. *Mater. Lett.* **2014**, *119*, 24−27.
(34) Metoki, N.; Liu, L.; Beilis, E.; Eliaz, N.; Mandler, D. *Langmuir* **2014**, *30*, 6791−6799.
(35) Ruiterkamp, G. J.; Hempenius, M. A.; Wormeester, H.; Vancso, G. J. *J. Nanopart. Res.* **2011**, *13*, 2779−2790.
(36) http://staff.aub.edu.lb/~tg02/IR.pdf. Last accessed 05/04/16.
(37) Xia, W.; Lindahl, C.; Lausmaa, J.; Engqvist, H. In *Advances in Biomimetics*; George, A., Ed.; InTech: India, 2011; Chapter 20, pp 429−452.
(38) Uchida, M.; Kim, H. M.; Kokubo, T.; Fujibayashi, S.; Nakamura, T. *J. Biomed. Mater. Res.* **2003**, *64*, 164−170.
(39) Schönherr, H.; Vancso, G. J. *Langmuir* **1997**, *13*, 3769−3774.
(40) Eliaz, N.; Kopelovitch, W.; Burstein, L.; Kobayashi, E.; Hanawa, T. *J. Biomed. Mater. Res., Part A* **2009**, *89*, 270−280.
(41) Larsen, M. J.; Jensen, S. J. *Arch. Oral Biol.* **1989**, *34*, 957−961.
(42) Liu, Z. X.; Wang, X. M.; Wang, Q.; Shen, X. C.; Liang, H.; Cui, F. Z. *CrystEngComm* **2012**, *14*, 6695−6701.
(43) Wu, D. J.; Liu, Z. X.; Gao, C. Z.; Shen, X. C.; Wang, X. M.; Liang, H. *Surf. Coat. Technol.* **2013**, *228*, S24−S27.
(44) Lu, H. B.; Campbell, C. T.; Graham, D. J.; Ratner, B. D. *Anal. Chem.* **2000**, *72*, 2886−2894.
(45) LeGeros, R. Z. *Calcif. Tissue Int.* **1985**, *37*, 194−197.
(46) Cavalleri, O.; Gilbert, S. E.; Kern, K. *Chem. Phys. Lett.* **1997**, *269*, 479−484.

DOI: 10.1021/acs.cgd.6b00057
Cryst. Growth Des. 2016, 16, 2756−2764